2-14-2020

Evidence of paracrystalline cation order in the Ruddlesden-Popper phase LaSr3NiRuO8 through total scattering techniques

Margaret Lea Robinson

Ernestine Whitaker

Lun Jin

Michael A. Hayward

Geneva Laurita
Bates College, glaurita@bates.edu

Recommended Citation

M. L. Robinson, E. Whitaker, L. Jin, M. A. Hayward, and G. Laurita, Evidence of paracrystalline cation order in the Ruddlesden-Popper phase LaSr3NiRuO8 through total scattering techniques. Inorganic Chemistry. 59 (2020) 3026-3033. https://doi.org/10.1021/acs.inorgchem.9b03382

Evidence of paracrystalline cation order in the Ruddlesden-Popper phase $LaSr_3NiRuO_8$ through neutron total scattering techniques

Margaret Lea Robinson,[†] Ernestine Whitaker,[†] Lun Jin,[‡] Michael A. Hayward,[‡] and Geneva Laurita[*,†]

†*Department of Chemistry and Biochemistry, Bates College, Lewiston, ME*

‡*Department of Chemistry, University of Oxford, Inorganic Chemistry Laboratory, South Parks Road, Oxford, OX1 3QR, U.K.*

E-mail: glaurita@bates.edu

Abstract

Cation ordering in perovskite-derived phases can lead to a wealth of tunable physical properties. Ordering is typically driven by a large difference between cation size or charge, but many Ruddlesden-Popper phases $A_{n+1}B_nO_{3n+1}$ appear to lack such B-site ordering, even when these differences are present. One such example is the 'double' Ruddlesden-Popper n=1 composition $LaSr_3NiRuO_8$. In this material, lack of B-site ordering is observed through traditional crystallographic techniques, but antiferromagnetic ordering in the magnetism data suggests B-site cation ordering is indeed present. Neutron total scattering, particularly analysis of the neutron pair distribution function, reveals the structure is locally B-site ordered below 6 Å, but becomes slightly disordered in the mid-range structure around 12 Å. This provides evidence for paracrystalline order in this material: cation ordering within a single perovskite sheet that lacks perfect registry within the 3-dimensional stack of sheets. This work highlights the importance of employing a structural technique that can probe both the local and mid-range order in addition to the crystallographic structure, and provides a structural origin to the observed magnetic properties of $LaSr_3NiRuO_8$. Further, it is proposed that paracrystalline order is likely to be common amongst these layered-typed oxides.

Introduction

The ABO_3 perovskite structure is almost ubiquitous in mixed-metal oxide chemistry.[1] This is largely because the mechanical flexibility of the network of apex-linked BO_6 octahedra which constitutes the perovskite framework leads to a high level of chemical flexibility, enabling almost all the transition metals to be accommodated within perovskite oxide phases. As a result, chemists have numerous opportunities to modify the chemical compositions of perovskite oxide materials by substituting some or all of the A- or B-site cations. These substitutions can modify the electron counts/valence states of metals, and/or adjust the subtle collective structural distortions of the perovskite network, which in turn can rationally tune the physical and chemical properties of these materials.[2]

A further feature which can be utilized to change the physical behavior of perovskite oxides is cation order. The most common cation ordered formulations are the $AA'B_2O_6$ and $A_2BB'O_6$ double perovskites which exhibit A- and B-cation ordering respectively.[3] There is much interest in these cation-ordered phases because they can have physical and chemical behaviors which are strikingly different to cation-disordered analogues. For example, A-cation ordered $LaBaMn_2O_6$ is observed to have a much higher ferromagnetic ordering temperature than the A-cation disordered analogue $La_{0.5}Ba_{0.5}MnO_3$,[4] while the tunneling magnetoresistance observed in samples of Sr_2FeMoO_6 is extremely sensitive to the degree of Fe/Mo B-site order present in the phase.[5]

It has generally been observed that B-site cation-ordered perovskite phases only become stable with respect to disordered analogues when there is a significant charge difference between the cations to be ordered.[6] Typically a difference of 3 charge units or more is required to stabilize cation ordered perovskite structures, although this requirement can be softened if there is a large difference in size between cations or if they have different local coordination preferences. More subtle features such as the tilting distortions of a phase or local Jahn-Teller distortions can add to the charge/size difference to influence the arrangement the ordered cations adopt,[3] and by appreciating these features, chemists have

been able to prepare a large and ever-expanding list of cation-ordered perovskite oxides.[7]

Layered variants of the perovskite structure, such as $A_{n+1}B_nO_{3n+1}$ Ruddlesden-Popper phases (n =1 illustrated in Figure 1a), can in principle exhibit an analogous ordering of cations to that seen in the $n = \infty$ perovskite oxides. However, while there are many examples of A-site cation-ordered Ruddlesden-Popper phases (most based on segregation of cations between 9- and 12-coordinate A-sites) there are relatively few which exhibit B-site cation order. This dearth of B-site ordered Ruddlesden-Popper phases is particularly surprising given that there are numerous examples of phases with suitable compositions to exhibit 1:1 B-site order (i.e. $A_2B_{0.5}B'_{0.5}O_4$) with charge differences between the B and B' cations of greater than 2 units, and for which the corresponding $A_2BB'O_6$ perovskite phase adopts a cation ordered structure.

One explanation of the dearth of B-site cation ordered Ruddlesden-Popper phases can be found in the observation that low concentrations of stacking faults can mask the signatures of B-site cation order in conventional X-ray and neutron powder diffraction data. This effect can clearly be seen in the Li/Ru and Li/Mn series of "double" Ruddlesden-Popper oxides. $La_2Sr_2LiRuO_8$ adopts a structure with rigorous A-site La/Sr and B-site Li/Ru cation order, which can be readily deduced from both X-ray and neutron powder diffraction data, and confirmed by ^{7}Li MAS NMR and HRTEM imaging.[8] In contrast X-ray and neutron powder diffraction data collected from La_4LiMnO_8 and $La_3SrLiMnO_8$ show no evidence for B-site Li/Mn cation order.[9] However a combination of ^{7}Li MAS-NMR and HRTEM images reveal that both phases exhibit Mn/Li B-site cation-ordered sheets, analogous to the Li/Ru ordered sheets in $La_2Sr_2LiRuO_8$, but show no registry in the positions of the Li and Mn positions between neighboring perovskite layers, as illustrated in Figure 1b. La_4LiMnO_8 and $La_3SrLiMnO_8$ thus exhibit rigorous intralayer cation order, but almost no interlayer cation order. The Li/Mn cation order in these phases can therefore be considered to be 2-dimensional rather than 3-dimensional, a situation dubbed "paracrystalline" order.[9] Similar B-site paracrystalline order has also been observed for $La_2Sr_2MgMnO_8$ and

$La_2Sr_2ZnMnO_8$.[10]

It is likely that this type of paracrystalline order is common in A_4BB'O_8 "double" Ruddlesden-Popper phases because the defect energy associated with faults in the stacking of B/B' cation-ordered sheets is likely to be low. This low defect energy can be rationalized by noting that the relative ($\frac{1}{2}$,$\frac{1}{2}$, z) shift between adjacent perovskite sheets in the Ruddlesden-Popper structure (Figure 1a) means that while at first sight it appears there are two choices (P and Q shown in Figure 1c) when stacking two B-site cation ordered perovskite sheets, these two configurations are in fact equivalent. This is because each (B/B')O_6 unit in the top sheet lies above a square hole in the bottom sheet made from 2 BO_6 and 2 B'O_6 units, as shown in Figure 1c. As a result the two configurations P and Q are simply related by a 90° rotation around the stacking axis. The difference between a rigorously 3-dimensionally B-cation ordered phase (e.g. $La_2Sr_2LiRuO_8$)[8] and a paracrystalline ordered phase (e.g. Li_4MnLiO_8)[9] arises from the registry between the positions of the B and B' cations in the next-nearest perovskite layers. These next-nearest layers are rather remote from each other so typically any stabilizing/destabilizing interactions are going to be weak and thus the energy difference between stacking configurations R and R', shown in Figure 1d will be small. We can therefore conclude that it is likely that many A_4BB'O_8 "double" Ruddlesden-Popper phases will exhibit paracrystalline B-cation order, and given the lack of any strong signature in conventional powder diffraction data, it is likely that paracrystalline order is present in many candidate phases already reported in the literature.

One such candidate phase is $LaSr_3NiRuO_8$ – a compound reported recently as part of work looking at the preparation of transition-metal oxyhydride phases.[11] $LaSr_3NiRuO_8$ is observed by synchrotron X-ray powder diffraction to adopt a simple $n = 1$ Ruddlesden-Popper structure, with A-site cation disorder and no indication of B-site cation order in the diffraction data. However the expected transition metal oxidation state combination of Ni^{2+} and Ru^{5+} yields a 3 unit charge difference which should favor Ni/Ru order, and the corresponding perovskite phase, $LaSrNiRuO_6$, does adopt a B-site cation ordered double perovskite

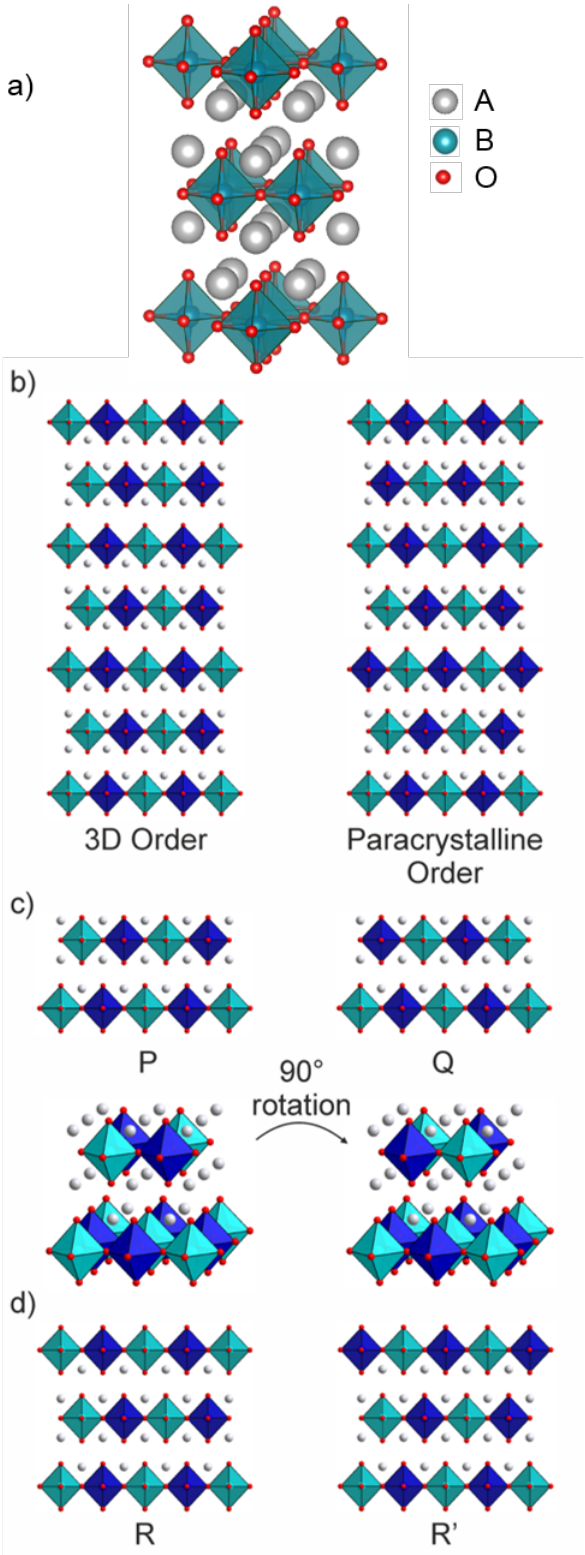

Figure 1: a) The A_2BO_4, $n = 1$ Ruddlesden-Popper structure. b) Arrangement of B-cations (dark and light blue) in 3D ordered and 2D "paracrystalline" ordered phases. c) Configurations P and Q of two stacked B-cation ordered sheets are equivalent, related by a 90° rotation. d) 3D B-cation order is determined by the registry between B-cations in next-nearest layers.

structure.[12,13] Furthermore, analysis of the magnetic couplings present in $LaSrNiRuO_6$[11,13,14] suggest that a disordered arrangement of Ni^{2+} and Ru^{5+} should exhibit spin glass behavior, but $LaSr_3NiRuO_8$ appears to be antiferromagnetically ordered at low temperatures, in common with *B*-cation ordered $LaSrNiRuO_6$.[13] We have therefore conducted a neutron total scattering study to investigate the Ni/Ru *B*-site cation order in $LaSr_3NiRuO_8$. Our study indicates that the local structure is well described by Ni-Ru order within a layer, whereas the mid-range structure points to small deviations from cation ordering. This work highlights the importance of utilizing local and mid-range structural probes to gain a complete understanding of the structure-property relationships in a material, particularly in the context of properties that arise from multiple length scale interactions such as magnetic ordering.

Experimental

Sample Preparation and Characterization

Synthesis. Samples of $LaSr_3NiRuO_8$ were prepared by a high-temperature ceramic method. Suitable stoichiometric ratios of La_2O_3 (99.999%, dried at 900°C), $SrCO_3$ (99.994%), RuO_2 (99.99%, dried at 800°C) and NiO (99.998%) were ground together using an agate mortar and pestle, transferred into an alumina crucible, and then heated at a rate of 1°C min^{-1} to 1000°C in air to decompose the carbonate. The sample was then reground, pressed into pellets and then heated for 3 periods of 48 hours at 1300°C in air, with grinding between heating periods.

Characterization. High-resolution synchrotron X-ray powder diffraction (SXRD) data were collected using instrument I11 at the Diamond Light Source Ltd. Diffraction patterns were collected using Si-calibrated X-rays with an approximate wavelength 0.825 Å, from samples sealed in 0.3 mm diameter borosilicate glass capillaries. Neutron powder diffraction (NPD) data were collected using the D2b instrument (ILL, France) using a wavelength of $\lambda = 1.5943$ Å from samples contained within vanadium cans. Rietveld profile refinements

were performed using the GSAS suite of programs.[15,16] Time of flight (TOF) neutron total scattering data were collected on a powdered sample of $LaSr_3NiRuO_8$ on the NOMAD instrument located at the Spallation Neutron Source, Oak Ridge National Laboratory.[17] The sample was loaded in a vanadium can, and data were collected at ambient temperature for approximately 2 hours. The pair distribution function (PDF), $G(r)$, was obtained by the transformation of the total scattering function, $S(Q)$, according to the equation:

$$g(r) - 1 = \frac{1}{2\pi^2 r \rho \Sigma b^2} \int_{Q_{min}}^{Q_{max}} (S(Q) - 1) Q sin(Qr) dQ \quad (1)$$

where r is the peak position in Å, ρ is the number density in atoms per Å^3, b is the coherent neutron scattering length of each atom in barns, Q is the magnitude of the scattering vector in Å^{-1}, $G(r) = [g(r) - 1]$, $Q_{min} = 0.5$ Å, and $Q_{max} = 40$ Å^{-1} utilizing the *Mantid* software framework.[18,19] This range was selected to balance between resolution and termination ripples in the reduced data. Least squares refinements were performed on the data using the PDFgui software suite,[20] using Q_{broad} and Q_{damp} as obtained from a Si standard, and modeling correlated motion within the system using the delta-2 parameter. Crystal structures were visualized using the VESTA software suite.[21] DC magnetization data were collected using a Quantum Design MPMS SQUID magnetometer.

Results and Discussion

To verify phase purity and the average, crystalline structure of $LaSr_3NiRuO_8$, a series of diffraction experiments were performed on the material using various structural probes: synchrotron X-ray, constant wavelength (CW) neutron, and TOF neutron. A summary of the refined synchrotron and CW neutron diffraction data can be found in Tables 1 and 2, and Figure 2 summarizes the refined fits of these sets of data. Synchrotron and CW neutron analysis do not indicate 3-dimensional ordering of the B-site cations, as this would be evidenced by an expansion of the lattice with respect to disordered cations. However,

Table 1: Structural parameters from the refinement $LaSr_3NiRuO_8$ against synchrotron X-ray powder diffraction data.

	x	y	z	Fraction	U_{iso} (Å^2)
La/Sr (1)	0	0	0.35709(2)	0.25/0.75	0.0090(1)
Ni/Ru (1)	0	0	0	0.5/0.5	0.0040(2)
O (1)	0	0	0.1656(1)	1	0.0133(4)
O (2)	$\frac{1}{2}$	0	0	1	0.0060(6)
$LaSr_3NiRuO_8$ space group $I4/mmm$ (#139)					
Formula weight : 689.53 g mol^{-1}, $Z = 2$					
$a = 3.8904(1)$ Å, $c = 12.6297(1)$ Å, Volume = 191.16(1) Å^3					
Radiation source: Synchrotron X-ray, $\lambda = 0.82626(1)$ Å					
Temperature: 298 K					
$\chi^2 = 9.87$; R_{wp}= 5.67%;R$_p$ = 3.63%					

Table 2: Structural parameters from the refinement $LaSr_3NiRuO_8$ against monochromatic CW neutron powder diffraction data.

	x	y	z	Fraction	U_{iso} (Å^2)
La/Sr (1)	0	0	0.3569(1)	0.25/0.75	0.0032(1)
Ni/Ru (1)	0	0	0	0.5/0.5	0.0015(2)
O (1)	0	0	0.1637(1)	1	0.0049(3)
O (2)	$\frac{1}{2}$	0	0	1	0.0097(2)
$LaSr_3NiRuO_8$ space group $I4/mmm$ (#139)					
Formula weight : 689.53 g mol^{-1}, $Z = 2$					
$a = 3.88945(5)$ Å, $c = 12.6266(2)$ Å, Volume = 191.015(7) Å^3					
Radiation source: monochromatic neutrons, $\lambda = 1.5942$ Å					
Temperature: 298 K					
$\chi^2 = 7.014$; R_{wp}= 6.36%;R$_p$ = 4.75%					

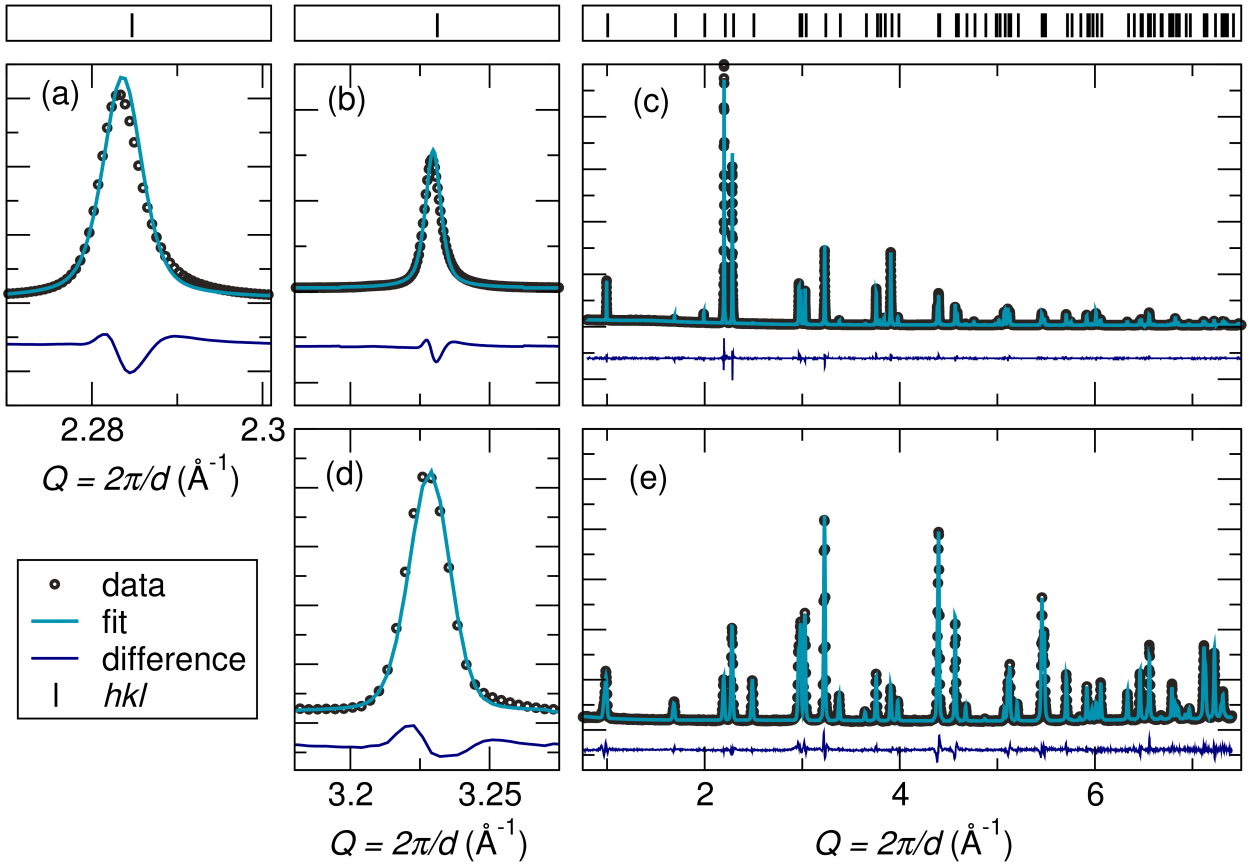

Figure 2: Observed, calculated and difference plots from the structural refinement of a cation disordered model of $LaSr_3NiRuO_8$ against (a, b, c) synchrotron X-ray powder diffraction data and (d, e) constant-wavelength neutron data. (a, b) Plots show poor fitting of (110) and (200) reflections in the X-ray data, and (d) shows poor fitting of the (200) reflection of the neutron data.

several peaks of index ($hk0$) exhibit peak tailing, (Figure 2a, b, and d) suggesting additional complexity in the stacking of the perovskite sheets, given the miller indices of the affected reflections. Neutron TOF data (from the total scattering experiment) were also fit with the refined CW neutron structure, and is in good agreement (R_{wp} = 6.84% for bank 4 of NOMAD data). Peak tailing was not investigated in this data set due to the complex profile shape of TOF peaks.

Zero-field cooled (ZFC) and field-cooled (FC) magnetization data collected from $LaSr_3NiRuO_8$ in an applied field of 100 Oe (Figure 3a) diverge below a temperature of approximately 50 K, with the ZFC data exhibiting a maximum at a temperature of approximately 30 K. Magnetization-field data collected at 5 K after cooling in a 50,000 Oe applied field (Figure 3b) show hysteresis, but crucially, are symmetric about the origin. This combination of magnetic behavior is characteristic of a canted antiferromagnet, and is incompatible with spin-glass behavior, for which a displaced magnetization-field response is expected. Considering the magnetic exchange interactions between Ni and Ru cations, the antiferromagnetic behavior observed for $LaSr_3NiRuO_8$ is incompatible with a disordered arrangement of the metals, and instead suggests an ordered Ni/Ru configuration. However, this contradicts the crystallographic structure obtained through diffraction analysis. We therefore performed a more detailed structural analysis to resolve this apparent paradox.

To investigate the possibility of cation ordering over various length scales and to elucidate the origin of the observed antiferromagnetic behavior, neutron total scattering was employed and analyzed through the atomic pair distribution function (PDF). The PDF is a histogram of all of the atom-atom correlations in a material, $G(r)$, and can provide insight on the local and mid-range atomic interactions. In the context of $LaSr_3NiRuO_8$, this technique provides crucial insight on cation ordering within the perovskite layers (local interactions), as well as registry between adjacent and next-nearest neighbor layers (mid-range correlations). The use of neutrons as a scattering probe provides contrast between the oxygen and metal atoms in the system, as well as good contrast between the Ni and Ru atoms in question (13.3 barn

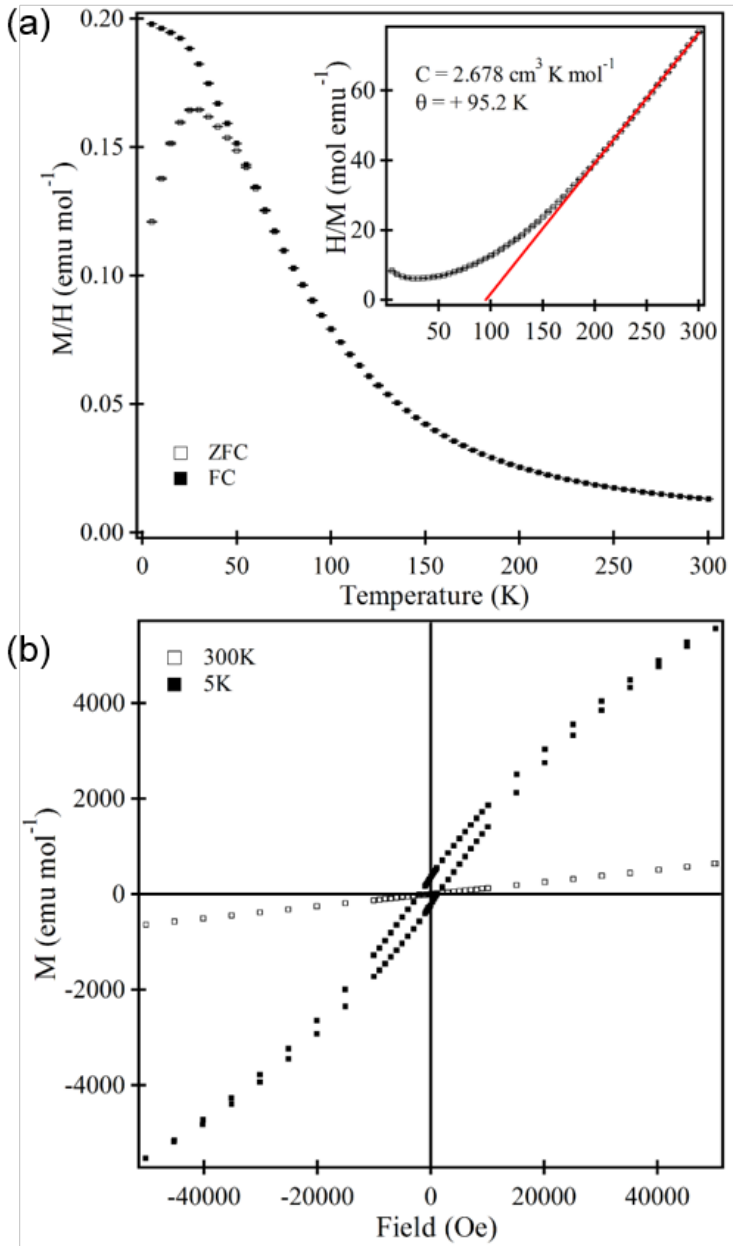

Figure 3: (a) Zero-field cooled and field-cooled magnetization data collected from $LaSr_3NiRuO_8$ in an applied filed of 100 Oe. (b) Magnetization-field isotherms collected from $LaSr_3NiRuO_8$ at 5 K and 300 K.

and 6.21 barn coherent neutron scattering cross sections, respectively[22]).

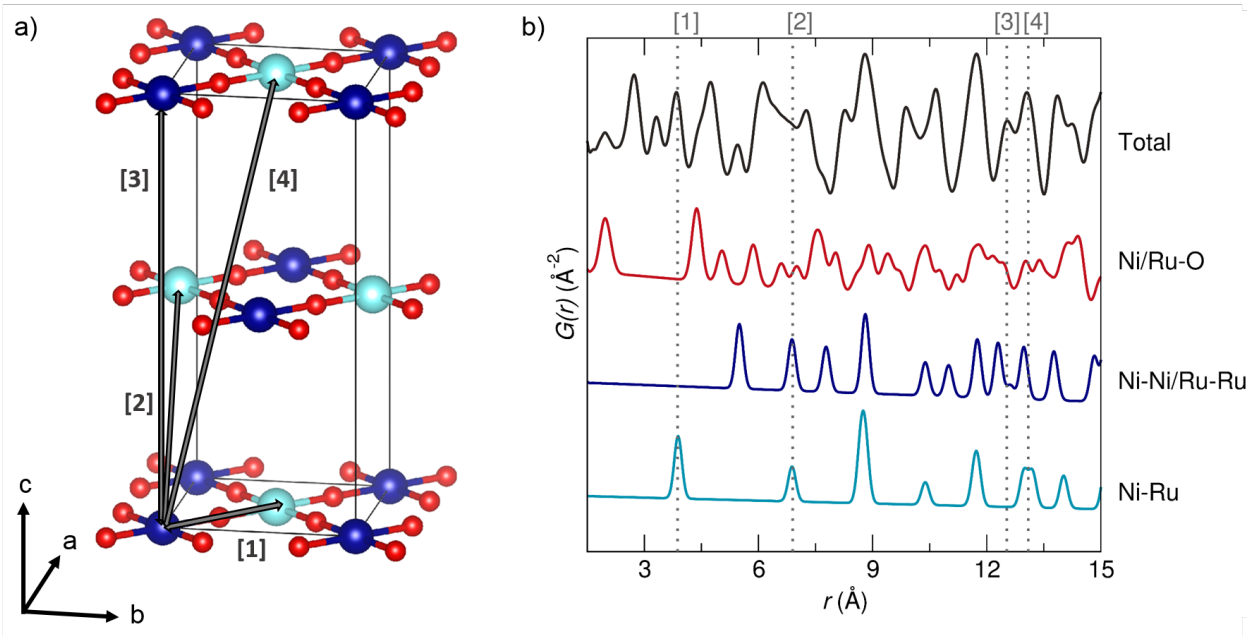

Figure 4: (a) Representative B cation correlations that illustrate [1] a Ni-Ru correlation within the same layer, [2] a Ni-Ru correlation between adjacent layers, and [3,4] a Ni-Ru correlation between next-nearest layers. (b) A comparison between the total PDF and Ni/Ru dependent partials. Dashed lines indicate [1], [2], [3], and [4] correlations indicated in (a).

Figure 4 illustrates the total calculated PDF for a fully 3D ordered $n = 1$ Ruddlesden Popper phase of $LaSr_3NiRuO_8$, along with various Ni- and Ru-dependent partial contributions. The partial correlations illustrate that the first intralayer Ni-Ru correlation can be found at approximately 3.9 Å, the first interlayer Ni-Ru correlation at approximately 6.8 Å, and the first next-nearest Ni-Ni and Ni-Ru correlations at approximately 12.5 and 13.0 Å, respectively. Knowledge of the locations of these partials can help guide our analysis when comparing the cation ordering across the material: ordering within a layer is best characterized using a local range between 1 and 10 Å, whereas the investigation of the existence of "paracrystalline" order and next-nearest registry requires a mid-range analysis over 10 to 25 Å.

As indicated by Figure 4, the regions in the PDF that indicate paracrystalline order are the first Ni/Ru correlation within the same layer at approximately 3.7 Å and the Ni/Ru

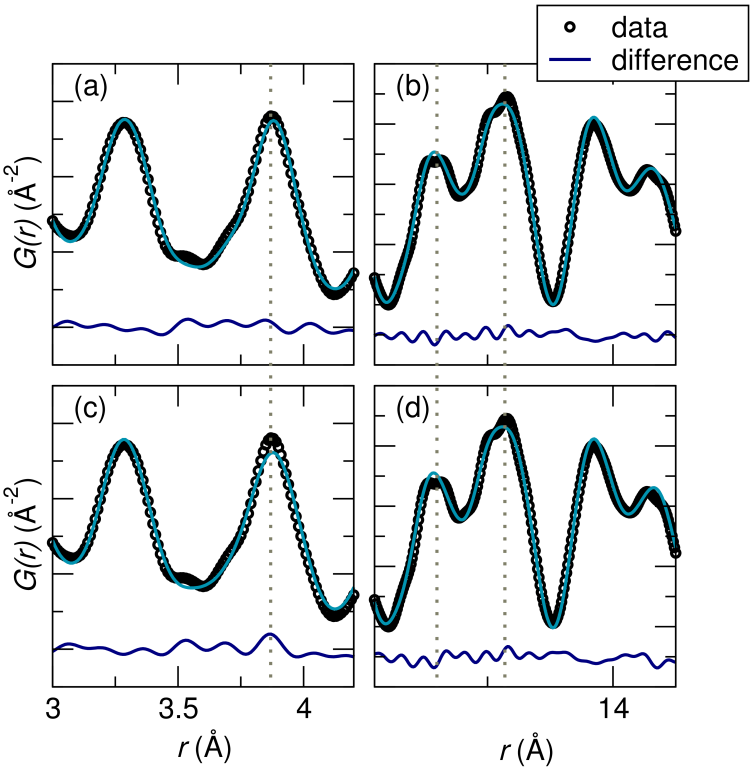

Figure 5: Comparison of the data fit against Ni/Ru ordered (a, b) and Ni/Ru disordered (c, d) models. The first Ni/Ru correlation, indicated by the dashed line at approximately 3.7 Å, is better fit by an ordered model ($R_w = 5.1\%$) than a disordered model ($R_w = 7.0\%$), whereas the the next-nearest neighbor, indicative of layer ordering, is fit moderately better by the ordered model than the disordered model ($R_w = 5.4$ and 6.5%, respectively).

correlations between next nearest layers between approximately 12.5 and 13.5 Å. Two initial models were constructed: the completely ordered model shown in Figure 4 and a completely disordered model, where Ni and Ru occupancy was set at 50% for all B sites. The two models were fit against the neutron PDF over a range of 1–5 Å and 10–15 Å, illustrated in Figure 5. Although there is good contrast between the scattering cross sections of Ni and Ru, the differences in the two models are subtle, primarily due to the combinations of Ni-Ni, Ru-Ru, and Ni-Ru correlations within a layer: in the ordered model, each Ni has 4 Ru neighbors and each Ru has 4 Ni neighbor, and in the disordered model, each Ni has an average of 2 Ni and 2 Ru neighbours, as does each Ru. Therefore, only four of the eight correlations will change between the models. Regardless of this small difference between the two models, a better description of the Ni/Ru correlation within the layer is obtained with the ordered model (Figure 5a), indicating the Ni and Ru cations are ordered within a single layer. A comparison of the two models against the data representative of the next nearest layers shows that the ordered model is still moderately a better fit than the disordered model, but it can be seen that there are clear misfits of data with both models, suggesting a completely ordered or disordered model are not accurate pictures of the next nearest neighbor layer, supporting the idea of paracrystallinity of this sample.

If an ordered modeled is assumed, a comparison of this model against various length-scales within the data can provide meaningful information about the extent or lack of ordering over a given data range. For example, a fit range of 1–5 Å is more representative of local coordination environments, while a fit range of 1–25 Å captures more atom-atom interactions and may more closely resemble the average, crystallographic structure. Neutron PDF data were fit against the B-site cation ordered $n = 1$ Ruddlesden-Popper phase of $LaSr_3NiRuO_8$ across various real-space distances (r = 1.7 – 25, 1.7 – 12.5, and 1.7 – 5 Å, shown in the right-hand panel of Figure 6 a, b, and c, respectively) to investigate the validity of cation ordering throughout the structure. In addition to various r distances, several types of "box-car" fits were performed up to a distance of r = 25 Å. "Box-car" fits are performed by

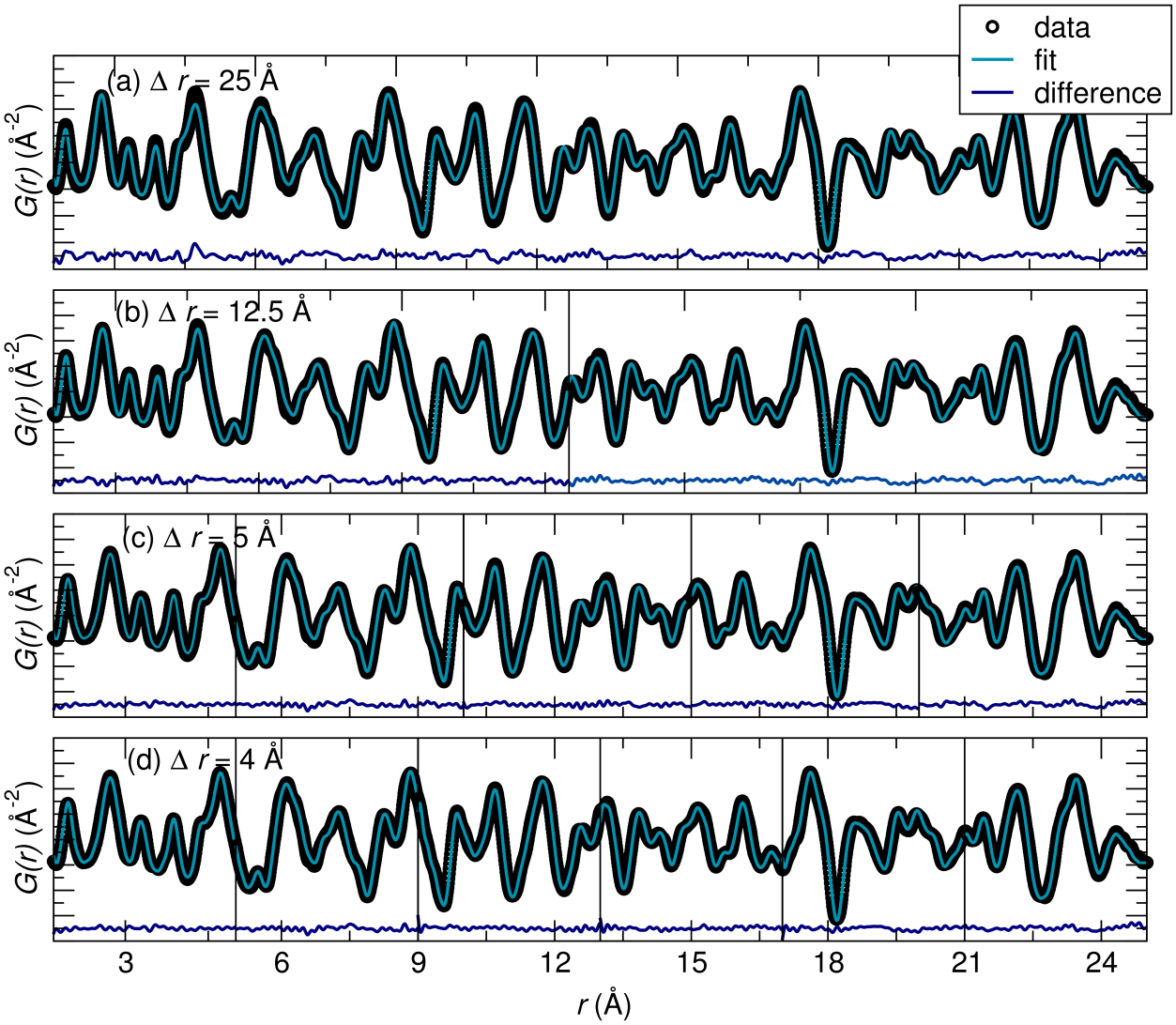

Figure 6: Fits of the neutron PDF data against various r-range increments (Δr) illustrates small deviations in the difference curves decrease with decreasing Δr, indicating there is some degree of correlation length dependence on the description of the atomic interactions.

taking a set r-range, for example, 5 Å, and fitting the data at various length scales with this range, for example 0–5 Å, 5–10 Å, 10–15 Å, etc., and can provide further insight on any r-dependent behaviour of the material. Our "box-car" comparisons (ranges illustrated by vertical solid lines in Figure 6) fit the data over a set r-range increment, Δr, up to a particular r maximum. The data were fit against the ordered structure with Δr increments of 25, 12.5, 5, and 4 Å to verify cation ordering within a layer (captured in the first Δr = 5 Å fit), between adjacent layers (captured in the first Δr = 12.5 Å fit), and between next-nearest neighbors (captured in the first Δr = 25 Å fit). An additional increment of Δr = 4 Å was tested to ensure fits over small r-ranges were representative of actual structural features, not artifacts of the fit range.

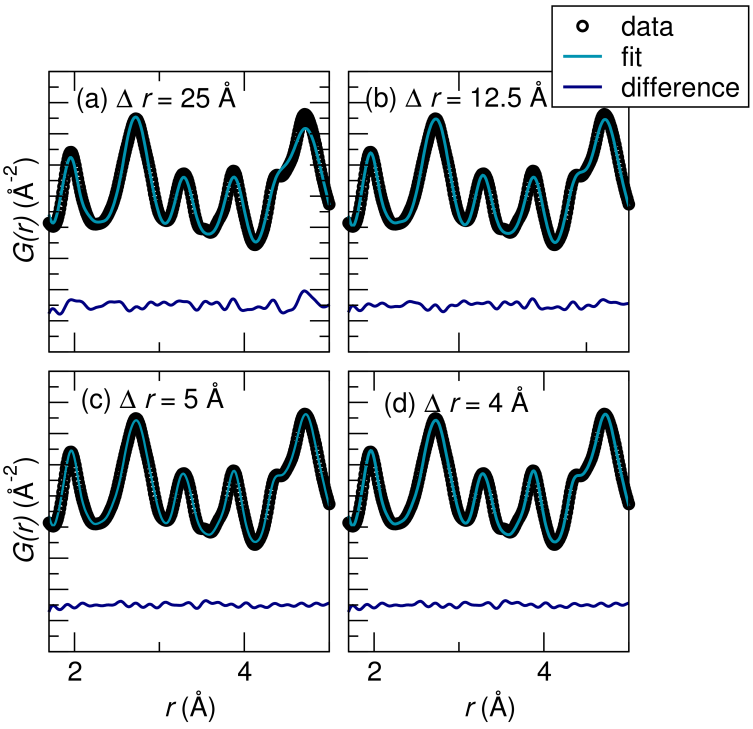

Figure 7: Fits from 1.7-5 Å obtained from various r-range increments (Δr) indicates a good description of the observed in-layer correlations, and the fit is further improved with a decreasing Δr.

Regardless of fit range, the data are fit well by the 3D B-site cation ordered model, with goodness-of-fit parameters R_w less than 10% for all fit ranges. This indicates that rather than the random Ni/Ru distribution, suggested by the average structure determined from

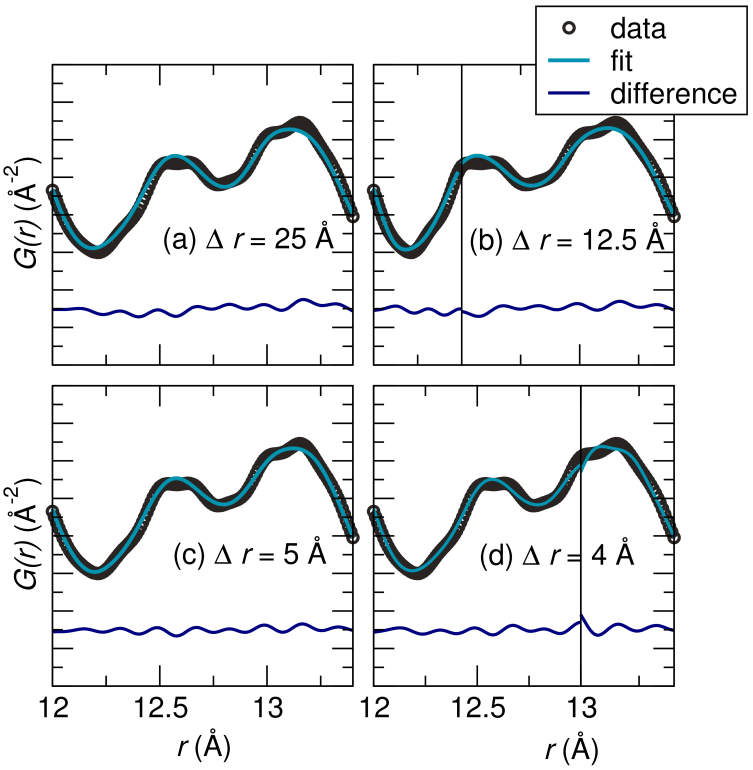

Figure 8: Fits from 12-15 Å obtained from various r-range increments (Δr) indicates a poor fit of the observed peak splitting in the next-nearest layer region of the data regardless of Δr.

SXRD and CW neutron diffraction data, $La_3SrNiRuO_8$ has a high level of B-site cation order. Fits against various Δr increments however, illustrate that the fit to the data is further improved with decreasing Δr values, indicated by flatter difference curves in Figure 6b, c, and d. Small deviations from the ordered model can be observed in several regions of the Δr = 25 Å fit (highlighted in Figures 7a and 8a) occurring around approximately 4.5 and 12 – 13 Å. The peak around 4.5 Å corresponds to La/Sr–O and O–O partials, and is independent of Ru/Ni ordering; however, the correlations between 12 and 13 Å correspond to next-nearest layer interactions. This indicates there are slight deviations from a completely ordered 3D structure: there appears to be good Ni/Ru ordering within the perovskite layers and extensive registry between adjacent nearest layers, but some degree of that registry is lost between next-nearest neighboring layers. Upon lowering Δr to 12.5, 5, or 4, a better fit is obtained for the peak around 4.5 Å (Figure 7b, c, and d), but a poor description of the peak splitting in the 12—13 Å region is still observed (Figure 8b, c, and d). Together, this indicates that while the long range La/Sr–O and O–O interactions can most likely be described by correlated atomic motion, the discrepancies between the fit and the data due to next-nearest layer interactions are indeed due to paracrystalline Ni/Ru order in the material.

Goodness-of-fit parameters R_w and B-site atomic displacement parameters (ADPs, modeled as U_{iso}) are shown as a function of r_{max} for the various Δr series in Figure 8. As observed from the fits of the data (Figure 6), a worsening of the fit of the data around 12 – 13 Å is observed with decreasing Δr. This is also supported by the evolution of U_{iso}, which is elevated in the Δr = 5 and 4 Å series around an r_{max} of 15 and 17 Å, respectively, indicating that there is some degree of disorder of this site when three layers are considered. This is opposed to one, two, or four layers, where the U_{iso} values of both cations are relatively low, further indicating there is minimal disorder present within a single layer or two neighboring layers.

The analysis of the PDF data described above reveals extensive Ni/Ru cation order in $LaSr_3NiRuO_8$, with fully 3D cation-ordered models only having small mismatches with the

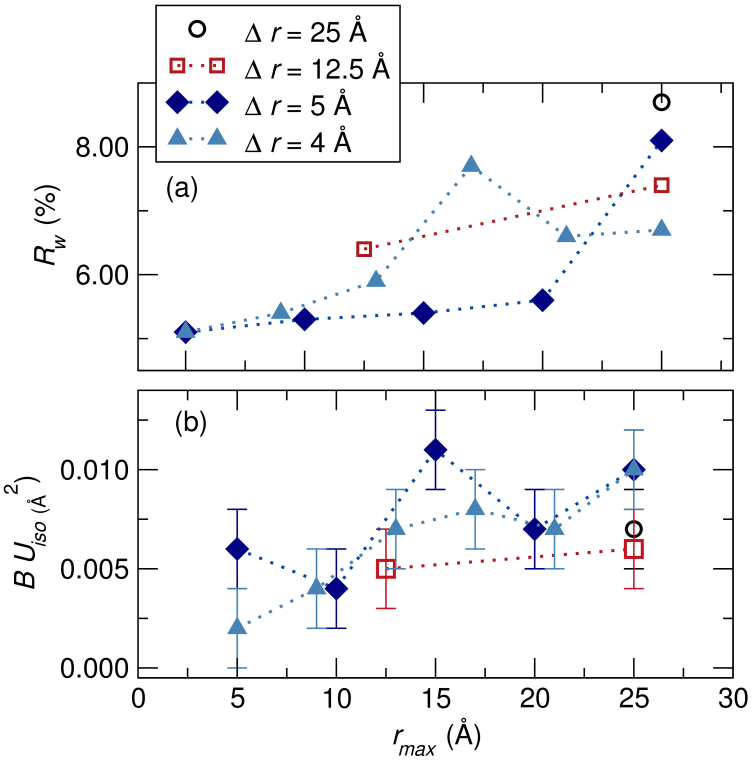

Figure 9: (a) R_w values obtained from fitting the neutron PDF data over various r-range increments (Δr) as a function of r_{max} illustrate that as Δr decreases, an apparent worsening of the fit (indicated by an elevated R_w) is observed over the next-nearest neighbor region of the PDF (approximately 12-13.5 Å). (b) Atomic displacement parameters, U_{iso}, of the B-site cations as a function of r_{max} for the various Δr series reveal an elevated U_{iso} in the next-nearest neighbor range (10-15 Å), suggesting disorder in this region.

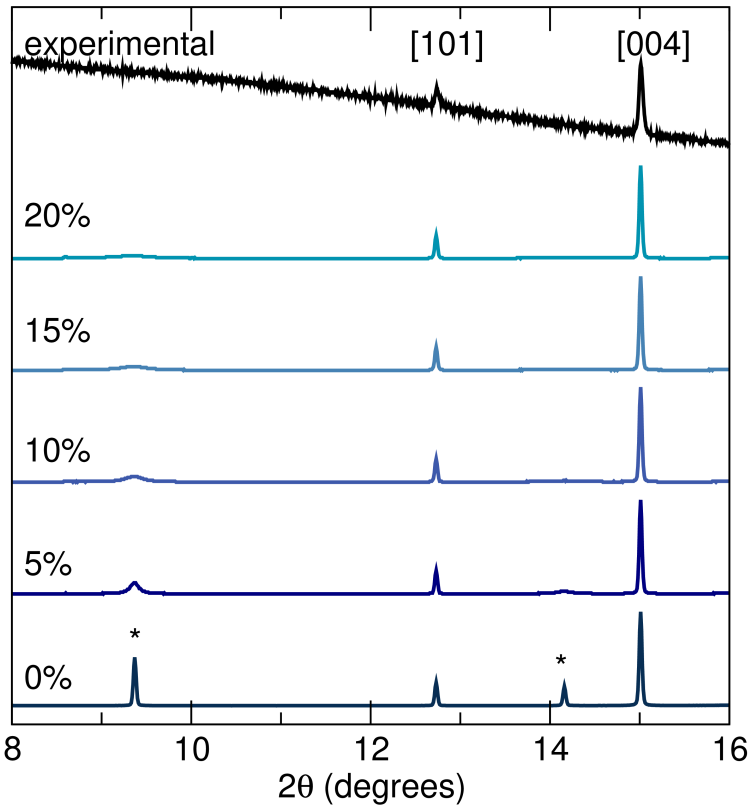

Figure 10: Calculated SXRD profiles for Ni/Ru cation-ordered structural models containing increasing concentrations of stacking faults. * indicates the location of supercell peaks indicative of 3D cation order. The experimental SXRD data collected from $LaSr_3NiRuO_8$ is also plotted for comparison.

observed data. It is therefore a bit of a surprise that there is no direct indication of cation order in the Rietveld fits to either the synchrotron X-ray or CW neutron diffraction data. To further investigate this apparent contradiction, we have performed a series of simulations using the FAULTS code[23] to assess the effect of stacking faults on the appearance of the supercell peaks which would be indicative of 3D Ni/Ru cation order.

Figure 10 shows a truncated range of the synchrotron X-ray diffraction pattern collected from $LaSr_3NiRuO_8$ compared with a series simulated diffraction patterns with differing concentrations of stacking faults. The bottom trace (0%) in Figure 10 shows the diffraction pattern expected for a fully 3D cation-ordered material, which in addition to the [101] and [004] reflections, exhibits 2 supercell diffraction peaks (marked with a star) consistent with an $a' = b' = \sqrt{2 * a}$ unit cell expansion. The traces above (5%-20%) show the influence of adding stacking faults of the type shown in Figure 1b, which disrupt the registry in the cation-order between perovskite sheets. A complete description of the FAULTS models is given in the Supporting Information. It can be seen that the introduction of small amounts of stacking disorder rapidly broadens the supercell reflections into the background so that at a stacking fault concentration of around 20% no supercell reflections are observable, and thus the data show no indication of Ni/Ru cation order although complete intralayer cation order is retained. This analysis shows that the appearance of supercell reflections indicative of B-site cation order is very sensitive to the presence of stacking disorder, so that materials with essentially perfect in-plane cation order can exhibit no observable supercell reflections when only modest concentrations of stacking faults are present.

Conclusions

Cation ordering can be a useful driver for functionality in a wide range of materials. As a consequence, a detailed understanding of the form and length-scale of any cation order present in a material can be decisive in achieving an accurate understanding of the underlying origin

of the material properties. In this work we have demonstrated that in systems with extensive 2D cation-order, but with stacking faults which limit the 3D cation order, conventional powder diffraction measurements to establish the average structure of materials can show no signature of the extensive cation order present, leading to the erroneous conclusion that the system is cation-disordered, even over short length-scales. This observation emphasizes the need to employ techniques that can provide information on the local-, mid-, and long-range order to accurately characterize materials, especially paracrystalline materials which exhibit extensive intra-layer cation order, but only limited inter-layer cation order.

In the specific case studied here, the observation of extensive intra-layer cation order allows us to understand the antiferromagnetic behavior of $LaSr_3NiRuO_8$ on the basis of the magnetic coupling interactions determined for the cation-ordered perovskite analogue $LaSrNiRuO_6$,[13] resolving the previous contradiction between an apparently cation-disordered structure (which should lead to spin-glass behavior) and the observed antiferromagnetic order.

Given that average structure determination by powder diffraction is typically the only structural characterization applied to most materials, it is likely that there are a large number of layered compounds in the literature that are currently assigned cation-disordered structures, but which in fact exhibit extensive paracrystalline cation order. By revealing this concealed cation-order, a better appreciation of the structure-property relations at play in these phases can be achieved, and new functionality potentially induced.

Acknowledgement

Acknowledgment is made to Bates College Sherman-Fairchild Summer Research Grant (MR, EW, and GL) for support of this research. This research used resources at the Spallation Neutron Source, a DOE Office of Science User Facility operated by the Oak Ridge National Laboratory. The authors would like to additionally thank Daniel Olds, Katharine Page, and

Michelle Everett for assistance with data collection and reduction during the experiment. We thank E. Suard for help with experiments at the ILL. We thank The Leverhulme Trust grant award RPG-2014-366 "Topochemical reduction of 4d and 5d transition metal oxides" for supporting this work. Experiments at the Diamond Light Source were performed as part of the Block Allocation Group award "Oxford Solid State Chemistry BAG to probe composition-structure-property relationships in solids" (EE13284).

Supporting Information Available

Structural information for the Faults simulation model.

References

(1) Tilley, R. J. D., *Perovskites: Structure-Property Relationships*, 2nd ed.; John Wiley & Sons. Ltd.: Chichester, 2016.

(2) Goodenough, J. B.; Zhou, J.-S. Localized to itinerant transition in transition metal oxides. *Chemistry of Materials* **1998**, *10*, 2980–2993.

(3) King, G.; Woodward, P. M. Cation Ordering in Perovskites. *Journal of Materials Chemistry* **2010**, *20*, 5785–5796.

(4) Millange, F.; Caignaert, V.; Domenges, B.; Raveau, B.; Suard, E. Order-disorder phenomena in new $LaBaMn_2O_{6-x}$ CMR perovskites. *Chemistry of Materials* **1998**, *10*, 1974.

(5) Meneghini, C.; Ray, S.; Liscio, F.; Bardelli, F.; Mobilio, S.; Sarma, D. D. Nature of the disorder in the ordered double perovskite Sr_2FeMoO_6. *Physical Review Letters* **2009**, *103*, 46403.

(6) Anderson, M. T.; Greenwood, K. B.; Taylor, G. A.; Poeppelmeier, K. R. B-cation arrangements in double perovskites. *Progress in Solid State Chemistry* **1993**, *22*, 197.

(7) Vasala, S.; Karppinen, M. $A_2B'B''O_6$ perovskites: a review. *Progress in Solid State Chemistry* **2015**, *43*, 1–36.

(8) Rodgers, J. A.; Battle, P. D.; Dupre, N.; Grey, C. P.; Sloan, J. Cation and spin ordering in the n = 1 Ruddlesden-Popper phase $La_2Sr_2LiRuO_8$. *Chemistry of Materials* **2004**, *16*, 4257–4266.

(9) Burley, J. C.; Battle, P. D.; Gallon, D. J.; Sloan, J.; Grey, C. P.; Rosseinsky, M. J. Magnetism and structural chemistry of the n = 1 Ruddlesden-Popper phases La_4LiMnO_8 and $La_3SrLiMnO_8$. *Journal of the American Chemical Society* **2002**, *124*, 620–628.

(10) Burley, J. C.; Battle, P. D.; Gaskell, P. J.; Rosseinsky, M. J. Structural and magnetic chemistry of $La_2Sr_2BMnO_8$ (B=Mg, Zn). *Journal of Solid State Chemistry* **2002**, *128*, 202–207.

(11) Jin, L.; Lane, M.; Zeng, D.; Kirschner, F. K. K.; Lang, F.; Manuel, P.; Blundell, S. J.; McGrady, J. E.; Hayward, M. A. $LaSr_3NiRuO_4H_4$: a 4d transition-metal oxide-hydride containing metal hydride sheets. *Angewandte Chemie International Edition* **2018**, *57*, 5025–5028.

(12) Gateshki, M.; Igartua, J. M. Crystal structures and phase transitions of the double perovskite oxides $SrLaCuRuO_6$ and $SrLaNiRuO_6$. *Materials Research Bulletin* **2003**, *38*, 1893–1900.

(13) Morrow, R.; McGuire, M. A.; Yan, J. Q.; Woodward, P. M. The Crystal Structure and Magnetic Behavior of Quinary Osmate and Ruthenate Double Perovskites $LaABB'O_6$ (A = Ca, Sr; B = Co, Ni; B' = Ru, Os). *Inorganic Chemistry* **2018**, *57*, 2989–3001.

(14) Ou, X. D.; Fan, F. R.; Chen, X. T.; Li, T.; Jiang, L. X.; Stroppa, A.; Ouyang, X. P.; Wu, H. Magnetic frustration in double perovskite LaSrNiRuO6. *Europhysics Letters* **2018**, *123*, 57003.

(15) Toby, B. H. EXPGUI , A Graphical User Interface for GSAS. *Journal of Applied Crystallography* **2001**, *34*, 210–213.

(16) Larson, A. C.; Von Dreele, R. B. General Structure Analysis System (GSAS). *Los Alamos National Laboratory Report* **1994**, *LAUR*, 89–748.

(17) Neuefeind, J.; Feygenson, M.; Carruth, J.; Hoffmann, R.; Chipley, K. K. Nuclear Instruments and Methods in Physics Research B The Nanoscale Ordered MAterials Diffractometer NOMAD at the Spallation Neutron Source SNS. *Nuclear Instruments and Methods in Physics Research* **2012**, *287*, 68–75.

(18) Arnold, O. et al. Mantid–Data analysis and visualization package for neutron scattering and μ SR experiments. *Nuclear Instruments and Methods in Physics Research Section A: Accelerators, Spectrometers, Detectors and Associated Equipment* **2014**, *764*, 156 – 166.

(19) Olds, D.; Saunders, C. N.; Peters, M.; Proffen, T.; Neuefeind, J.; Page, K. Precise implications for real-space pair distribution function modeling of effects intrinsic to modern time-of-flight neutron diffractometers. *Acta Crystallographica Section A* **2018**, *74*, 293–307.

(20) Farrow, C. L.; Juhas, P.; Liu, J. W.; Bryndin, D.; Božin, E. S.; Bloch, J.; Proffen, T.; Billinge, S. J. L. PDFfit2 and PDFgui: computer programs for studying nanostructure in crystals. *Journal of Physics Condensed Matter* **2007**, *19*, 335219.

(21) Momma, K.; Izumi, F. VESTA 3 for Three-Dimensional Visualization of Crystal, Volumetric and Morphology Data. *Journal of Applied Crystallography* **2011**, *44*, 1272–1276.

(22) Sears, V. F. Neutron scattering lengths and cross sections. *Neutron News* **1992**, *3*, 26–37.

(23) Casas-Cabanas, M.; Reynaud, M.; Rikarte, J.; Horbach, P.; Rodriguez-Carvajal, FAULTS: a program for refinement of structures with extended defects. *Journal of Applied Crystallography* **2016**, *49*, 2259–2269.

Graphical TOC Entry